Approximating the Integral Fréchet Distance

Anil Maheshwari
School of Computer Science
Carleton University
Ottawa, Canada K1S5B6
anil@scs.calreton.cs

Jörg-Rüdiger Sack
School of Computer Science
Carleton University
Ottawa, Canada K1S5B6
sack@scs.carleton.ca

Christian Scheffer
Department of Computer Science
TU Braunschweig
Mühlenpfordtstr. 23,
38106 Braunschweig, Germany
scheffer@ibr.cs.tu-bs.de

arXiv:1512.03359v1 [cs.CG] 10 Dec 2015

Abstract

A pseudo-polynomial time $(1+\varepsilon)$-approximation algorithm is presented for computing the integral and average Fréchet distance between two given polygonal curves T_1 and T_2. In particular, the running time is upper-bounded by $\mathcal{O}(\zeta^4 n^4/\varepsilon^2)$ where n is the complexity of T_1 and T_2 and ζ is the maximal ratio of the lengths of any pair of segments from T_1 and T_2. The Fréchet distance captures the minimal cost of a continuous deformation of T_1 into T_2 and vice versa and defines the cost of a deformation as the maximal distance between two points that are related. The integral Frchet distance defines the cost of a deformation as the integral of the distances between points that are related. The average Frchet distance is defined as the integral Frchet distance divided by the lengths of T_1 and T_2.

Furthermore, we give relations between weighted shortest paths inside a single parameter cell C and the monotone free space axis of C. As a result we present a simple construction of weighted shortest paths inside a parameter cell. Additionally, such a shortest path provides an optimal solution for the partial Fréchet similarity of segments for all leash lengths. These two aspects are related to each other and are of independent interest.

1 Introduction

Measuring similarity between geometric objects is a fundamental problem in many areas of science and engineering. Applications arise e.g., when studying animal behaviour, human movement, traffic management, surveillance and security, military and battlefield, sports scene analysis, and movement in abstract spaces [9, 10, 11]. Due to its practical relevance, the resulting algorithmic problem of curve matching has become one of the well-studied problems in computational geometry. One of the prominent measures of similarities between curves is given by the *Fréchet distance* and its variants. *Fréchet* measures have been applied e.g., in hand-writing recognition [14], protein structure alignment [12], and vehicle tracking [3].

In the well-known dog-leash metaphor, the (standard) *Fréchet distance* is described as follows: suppose a person walks a dog, while both have to move from the starting point to the ending point on their respective curves T_1 and T_2. The *Fréchet* distance is the minimum leash length required over all possible pairs of walks, if neither person nor dog is allowed to move backwards. Here, we see the *Fréchet distance* as capturing the cost of a continuous deformation of T_1 into T_2 and vice versa. (A deformation is required to maintain the order along T_1 and T_2.) A specific deformation induces a relation $R \subset T_1 \times T_2$ such that "$p \in T_1$ is deformed into $q \in T_2$". For $(p,q) \in R$ we say p *is related to* q and vice versa. The *Fréchet distance* defines the cost of a deformation as the maximal distance between two related points.

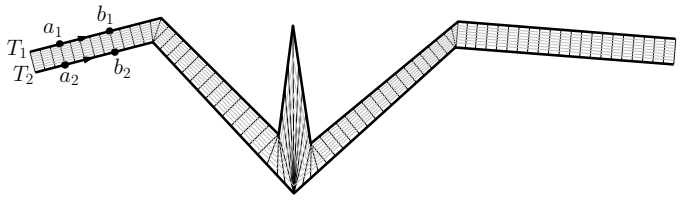

Figure 1: A deformation between T_1 and T_2 and the relation between T_1 and T_2. The deformation maintains the order of points along the curves. The distances between related points on the peak are larger than the distances between related points that do not lie on the peak.

In this paper, we study the integral and average Fréchet distance originally introduced by Buchin [6]. The *integral Fréchet distance* defines the cost of a deformation as the integral of the distances between points that are related. The *average Fréchet distance* is defined as the integral Fréchet distance divided by the lengths of T_1 and T_2. Next, we define these notions formally.

1.1 Problem Definition

Let $T_1, T_2 : [0, n] \to \mathbb{R}^2$ by two polygonal curves. We denote the first derivative of a function f by f'. By, $||\cdot||_p$, we denote the p-norm and by $d_p(\cdot,\cdot)$ its induced L_p metric. The *lengths* $|T_1|$ *and* $|T_2|$ of T_1 and T_2 are defined as $\int_0^n ||(T_1)'(t)||_2\, dt$ and $\int_0^n ||(T_2)'(t)||_2\, dt$, respectively. To simplify the exposition, we assume that $|T_1| = |T_2| = n$ and that T_1 and T_2 each have n segments. A *reparametrization* is a continuous function $\alpha : [0, n] \to [0, n]$ with $\alpha(0) = 0$ and $\alpha(n) = n$. A reparameterization α is *monotone* if $\alpha(t_1) \leqslant \alpha(t_2)$ holds for all $0 \leqslant t_1 \leqslant t_2 \leqslant n$. A *(monotone) matching* is a pair of (monotone) reparametrizations (α_1, α_2). The *Fréchet distance* of T_1 and T_2 w.r.t. d_2 is defined as $\mathcal{D}(T_1, T_2) = \inf_{(\alpha_1,\alpha_2)} \max_{t\in[0,n]} d_2(T_1(\alpha_1(t)), T_2(\alpha_2(t)))$.

For a given leash length $\delta \geqslant 0$, Buchin et al. [5] define the *partial Fréchet similarity* $\mathcal{P}_{(\alpha_1,\alpha_2)}(T_1, T_2)$ *w.r.t. a matching* (α_1, α_2) as

$$\int_{d_2(T_1(\alpha_1(t)),T_2(\alpha_2(t)))\leqslant\delta} \left(||\left(T_1 \circ \alpha_1\right)'(t)||_2 + ||\left(T_2 \circ \alpha_2\right)'(t)||_2\right) dt$$

and the *partial Fréchet similarity* as $\mathcal{P}_\delta(T_1, T_2) = \sup_{\alpha_1,\alpha_2} \mathcal{P}_{(\alpha_1,\alpha_2)}(T_1, T_2)$.

Given a monotone matching (α_1, α_2), the *integral Fréchet distance* $\mathcal{F}_{\mathcal{S},(\alpha_1,\alpha_2)}(T_1, T_2)$ *of* T_1 *and* T_2 *w.r.t.* (α_1, α_2) is defined as:

$$\int_0^n d_2(T_1(\alpha_1(t)), T_2(\alpha_2(t)))\left(||\left(T_1 \circ \alpha_1\right)'(t)||_2 + ||\left(T_2 \circ \alpha_2\right)'(t)||_2\right) dt$$

and the *integral Fréchet distance* as $\mathcal{F}_\mathcal{S}(T_1, T_2) = \inf_{(\alpha_1,\alpha_2)} \mathcal{F}_{\mathcal{S},(\alpha_1,\alpha_2)}(T_1, T_2)$ [6]. Note that the derivatives of $(T_1 \circ \alpha_1)(\cdot)$ and $(T_2 \circ \alpha_2)(\cdot)$ are measured w.r.t. the L_2-norm because the lengths of T_1 and T_2 are measured in Euclidean space. The *average Fréchet distance* is defined as $\mathcal{F}_S(T_1, T_2)/(|T_1| + |T_2|)$ [6].

While the integral Fréchet distance has been studied [3, p. 860], no efficient algorithm exists to compute this distance measure (see Subsection 1.2 for details). In this paper, we design the first pseudo-polynomial time algorithm for computing an $(1 + \varepsilon)$-approximation of the integral Fréchet distance and consequently of the average Fréchet distance.

1.2 Related Work

In their seminal paper, Alt and Godau [2] provided an algorithm that computes the Fréchet distance between two polygonal curves T_1 and T_2 in $\mathcal{O}(n^2 \log(n))$ time, where n is the complexity of T_1 and T_2. In the presence of outliers though, the Fréchet distance may not provide an appropriate result. This is due to the fact that the Fréchet distance measures the maximum of the distances between points that are related. This means that already one large "peak" may substantially increase the Fréchet distance between T_1 and T_2 when the remainder of T_1 and T_2 are similar to each other, see Figure 1 for an example.

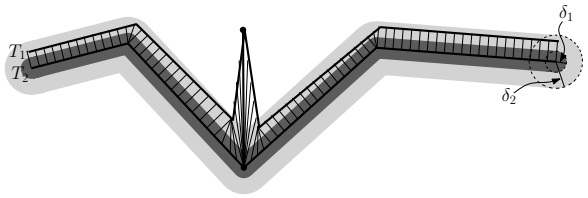

Figure 2: An optimal deformation between T_1 and T_2 for both, the Fréchet distance and the partial Fréchet similarity. Relative to the other portions, the Fréchet distance is significantly increased by the peak on T_1. The partial Fréchet similarity is unstable for distance thresholds between δ_1 and δ_2 where $\delta_1 \approx \delta_2$. The integral Fréchet distance between T_1 and T_2 is robust w.r.t. to small changes of the distances between related points and the influence of the peak.

To overcome the issue of outliers, Buchin et al. [5] introduced the notion of *partial Fréchet similarity* and gave an algorithm running in $\mathcal{O}(n^3 \log(n))$ time, where distances are measured w.r.t. the L_1 or L_∞ metric. The partial Fréchet similarity measures the cost of a deformation as the lengths of the parts of T_1 and T_2 which are made up of points that fulfill the following: The distances that are induced by straightly deforming points into their related points are upper-bounded by a given threshold $\delta \geqslant 0$, see Figure 2. De Carufel et al. [7] showed that the partial Fréchet similarity w.r.t. to the L_2 metric cannot be computed exactly over the rational numbers. Motivated by that, they gave an $(1 \pm \varepsilon)$-approximation algorithm guaranteeing a pseudo-polynomial running time. An alternative perspective on the partial Fréchet similarity is the partial Fréchet dissimilarity, i.e., the minimization of the portions on T_1 and T_2 which are involved in distances that are larger than δ. Observe that an exact solution for the similarity problem directly leads to an exact solution for the dissimilarity problem. In particular, the sum of both values is equal to the sum of the lengths of T_1 and T_2.

Unfortunately, both the partial Fréchet similarity and dissimilarity are highly dependent on the choice of δ as provided by the user. As a function of δ, the partial Fréchet distance is unstable, i.e., arbitrary small changes of δ can result in arbitrarily large changes of the partial Fréchet (dis)similarly, see Figure 2. In particular, noisy data may yield incorrect similarity results. For noisy data, the computation of the Fréchet distance in the presence of imprecise points has been explored in [1]. The idea behind this approach is to model signal errors by replacing each vertex p of the considered chain T_1 by a small ball centered at p. Unfortunately, the above described outlier-problem cannot be resolved by such an approach because the distance of an outlier to the other chain T_2 could be arbitrarily large. This would mean that the radii of the corresponding balls would have been chosen extremely large.

An approach related to the integral Fréchet distance is dynamic time warping (DTW), which arose in the context of speech recognition [13]. Here, a discrete version of the integral Fréchet distance is computed via dynamic programming. This is not suitable for general curve matching

(see [8, p. 204]). Efrat et al. [8] worked out an extension of the idea of DTW to a continuous version. In particular, they compute shortest path distances on a combinatorial piecewise linear 2-manifold that is constructed by taking the Minkowski sum of T_1 and T_2. Furthermore, they gave two approaches dealing with that manifold. The first one does not yield an approximation of the integral Fréchet distance. The second one does not lead to theoretically provable guarantees regarding both: polynomial running time and approximation quality of the integral Fréchet distance.

More specifically, [8] designed two approaches for continuous curve matching by computing shortest paths on a combinatorial piecewise linear 2-manifold $\mathcal{M}(T_1, T_2) := T_1 \ominus T_2 := \{T_1(\mu) - T_2(\lambda) | \lambda, \mu \in [0, n]\}$. In particular, they consider shortest path lengths between the points $T_1(0) - T_2(0)$ and $T_1(n) - T_2(n)$ on the polyhedral structure which is induced by $\mathcal{M}(T_1, T_2)$. The first approach is to compute in polynomial time the unweighted monotone shortest path length on $\mathcal{M}(T_1, T_2)$ w.r.t. d_2. This approach does not take into account the weights in form of the considered leash length. Therefore, it does not yield an approximation of the integral Fréchet distance. In contrast to this, the second approach considers an arbitrarily chosen weight function f such that the minimum path integral over all connecting curves on $\mathcal{M}(T_1, T_2)$ is approximated. In terms of Fréchet distances, this approach is an approximation of the integral Fréchet distances as described next. By flattening and rectifying $\mathcal{M}(T_1, T_2)$, we have a representation of the parameter space in the space of T_1 and T_2, such that by setting $f = w$ and considering shortest path length w.r.t. d_1 instead of d_2, we obtain the problem setting of computing the integral Fréchet distance (the function w is defined in Section 2). However, to compute the weighted shortest path length on $\mathcal{M}(T_1, T_2)$, Efrat et al. apply the so-called *Fast Marching Method*, "to solve the Eikonal equation numerically" [8, p. 211]. While "the solution it (ed.: the algorithm) provides converges monotonically" [8, p. 211], the solution does not give a $(1 + \varepsilon)$ approximation with pseudo-polynomial running-time.

1.3 Contributions

- We present a (pseudo-)polynomial time algorithm that approximates the integral Fréchet Distance, $\mathcal{F}_S(T_1, T_2)$, up to an multiplicative error of $(1 + \varepsilon)$. This measure is desirable because it integrates the inter-curve distances along the curve traversals, and is thus more stable (w.r.t. to the choice of δ) than other Fréchet Distance measures defined by the maximal such distance.

- The running time of our approach is $\mathcal{O}\left(\zeta^4 n^4 / \varepsilon^2 \log(\zeta n / \varepsilon)\right)$, where ζ is the maximal ratio of the lengths of any pair of segments from T_1 and T_2. Note that achieving a running time that is independent of $|T_1| + |T_2|$ seems to be quite challenging as $\mathcal{F}_S(T_1, T_2)$ could be arbitrary small compared to $|T_1| + |T_2|$.

- This guarantees an $(1 + \varepsilon)$ approximation within pseudo-polynomial running time which was not been achieved by the approach of [8].

- Our results thus answer the implicit question raised in [3]: "Unfortunately there is no algorithm known that computes the integral Fréchet distance."

- As a by-product, we show that a shortest weighted path π_{ab} between two points a and b inside a parameter cell C can be computed in constant time. We also make the observation that π_{ab} provides an optimal matching for the partial Fréchet similarity for all leash length thresholds. This provides a natural extension of locally correct Fréchet matchings that were first introduced by Buchin et al. [4]. They suggest to: "restrict to the locally correct matching

that decreases the matched distance as quickly as possible."[4, p. 237]. The matching induced by π_{ab} fulfils this requirement.

2 Preliminaries

The *parameter space* P of T_1 and T_2 is an axis aligned rectangle. The bottom-left corner $\mathfrak{s}$ and upper-right corner $\mathfrak{t}$ correspond to $(0,0)$ and (n,n), respectively. We denote the x- and the y-coordinate of a point $a \in P$ by $a.x$ and $a.y$, respectively. A point $b \in P$ *dominates* a point $a \in P$, denoted by $a \leqslant_{xy} b$, if $a.x \leqslant b.x$ and $a.y \leqslant b.y$ hold. A path π is *(xy-) monotone* if $\pi(t_1) \leqslant \pi(t_2)$ holds for all $0 \leqslant t_1 \leqslant t_2 \leqslant n$. Thus a monotone matching corresponds to a monotone path π with $\pi(0) = \mathfrak{s}$ and $\pi(n) = \mathfrak{t}$. By inserting $n+1$ vertical and $n+1$ horizontal *parameter lines*, we refine P into n rows and n columns such that the i-th row (column) has a height (resp., width) that corresponds to the length of the i-th segment on T_1 (resp., T_2). This induces a partitioning of P into cells, called *parameter cells*.

For $a, b \in P$ with $a \leqslant_{xy} b$, we have $||ab||_1 = \int_{a.x}^{b.x} ||(T_1)'(t)||_2 \, dt + \int_{a.y}^{b.y} ||(T_2)'(t)||_2 \, dt$. This is equal to the sum of the lengths of the subcurves between $T_1(a.x)$ and $T_1(b.x)$ and between $T_2(a.y)$ and $T_2(b.y)$. Thus, we define the *length* $|\pi|$ *of a path* $\pi : [0,n] \to P$ as $\int_0^n ||(\pi)'(t)||_1 \, dt$. Note that for the paths inside the parameter space the 1-norm is applied, while the lengths of the curves in the Euclidean space are measured w.r.t. the 2-norm. As $\mathcal{F}_S(T_1, T_2)$ measures the length of T_1 and T_2 at which each $(T_1(\alpha_1(t)), T_2(\alpha_2(t)))$ is weighted by $d_2(T_1(\alpha_1(t)), T_2(\alpha_2(t)))$, we consider the *weighted length* of π defined as follows:

Let $w(\cdot) : P \to \mathbb{R}_{\geqslant 0}$ be defined as $w((x,y)) := d_2(T_1(x), T_2(y))$ for all $(x,y) \in P$. The weighted length $|\pi|_w$ of a path $\pi : [a,b] \to P$ is defined as $\int_a^b w(\pi(t)) \, ||(\pi)'(t)||_1 dt$.

Observation 1 ([6]) *Let π be a shortest weighted monotone path between $\mathfrak{s}$ and $\mathfrak{t}$ inside P. Then, we have $|\pi|_w = \mathcal{F}_{\mathcal{S}}(T_1, T_2)$.*

Motivated by Observation 1, we approximate $\mathcal{F}_S(T_1, T_2)$ by approximating the length of a shortest weighted monotone path $\pi \subset P$ connecting $\mathfrak{s}$ and $\mathfrak{t}$. Let $\delta \geqslant 0$ be chosen arbitrarily but fixed. Inside each parameter cell C, the union of all points p with $w(p) \leqslant \delta$ is equal to the intersection of an ellipse $\mathcal{E}$ with C. Observe that $\mathcal{E}$ can be computed in constant time [2]. $\mathcal{E}$ is characterized by two focal points F_1 and F_2 and a radius r such that $\mathcal{E} = \{x \in \mathbb{R}^2 \mid d_2(x, F_1) + d_2(x, F_2) \leqslant r\}$. The two axes ℓ (monotone) and $\hbar$ (not monotone) of $\mathcal{E}$, called the *free space axes*, are defined as the line induced by F_1 and F_2 and the bisector between F_1 and F_2. If $\mathcal{E}$ is a disc, ℓ and $\hbar$ are the lines with gradients 1 and -1 and which cross each other in the middle of $\mathcal{E}$. Note that the axes are independent of the value of δ.

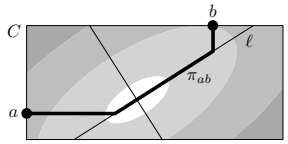

Figure 3: A weighted shortest xy-monotone path π_{ab} between two points $a, b \in C$, where $a \leqslant_{xy} b$. The subpaths of π_{ab} that do not lie on ℓ are minimal.

To approximate $|\pi|_w$ efficiently we make the following observation that is of independent interest: Let a, b be two parameter points that lie in the same parameter cell C such that $a \leqslant_{xy} b$. The shortest weighted monotone path π_{ab} between a and b (that induces an optimal solution for the

integral Fréchet distance) is the monotone path between a and b that maximizes its subpaths that lie on ℓ (see Figure 3 and Lemma 4). Another interesting aspect of π_{ab} is that it also provides an optimal matching for the partial Fréchet similarity (between the corresponding (sub-)segments) for all leash lengths, as $\pi \cap \mathcal{E}_\delta$ has the maximal length for all $\delta \geqslant 0$, where $\mathcal{E}_\delta := \mathcal{E}$ for a specific $\delta \geqslant 0$. Next, we discuss our algorithms.

3 An Algorithm for Approximating Integral Fréchet Distance

We approximate the length of a shortest weighted monotone path between $\mathfrak{s}$ and $\mathfrak{t}$ as follows: We construct two weighted, directed, geometric graphs $G_1 = (V_1, E_1, w_1)$ and $G_2 = (V_2, E_2, w_2)$ that lie embedded in P such that $\mathfrak{s}, \mathfrak{t} \in V_1$ and $\mathfrak{s}, \mathfrak{t} \in V_2$. Then, in parallel, we compute for G_1 and G_2 the lengths of the shortest weighted paths between $\mathfrak{s}$ and $\mathfrak{t}$. Finally, we output the minimum of both values as an approximation for $\mathcal{F}_S(T_1, T_2)$.

We introduce some additional terminology. A *geometric graph* $G = (V, E)$ is a graph where each $v \in V$ is assigned to a point $p_v \in P$, its *embedding*. The *embedding* of an edge $(u, v) \in E$ (into P) is $p_u p_v$. The *embedding of G (into P)* is $\bigcup_{(u,v)\in E} p_u p_v$. For $v \in V$ and $e \in E$, we denote simultaneously the vertex $v \in V$, the edge $e \in E$, and the graph (V, E) and their embeddings by v, e, and G, respectively. G is *monotone (directed)* if $p_u \leqslant_{xy} p_v$ holds for all $(u, v) \in E$. Let $R \subseteq P$ be an arbitrarily chosen axis aligned rectangle with height h and width b. The *grid (graph) of R with mesh size σ* is the geometric graph that is induced by the segments that are given as the intersections of R with the following lines: Let $h_1, \ldots, h_{k_1}$ be the $\lceil \frac{h}{\sigma} \rceil + 1$ equidistant horizontal lines and let $b_1, \ldots, b_{k_2}$ be the $\lceil \frac{b}{\sigma} \rceil + 1$ equidistant vertical lines such that $\partial R = R \cap (h_1 \cup h_{k_1} \cup b_1 \cup b_{k_2})$.

Construction of G_1: Let μ be the length of a smallest segment from T_1 and T_2. We construct $G_1 = (V_1, E_1) \subset P$ as the monotone directed grid graph of P with a mesh size of $\frac{\varepsilon\mu}{40000(|T_1|+|T_2|)}$. Furthermore, we set $w_1((u, v)) := |uv|_w$ for all $(u, v) \in E_1$.

Construction of G_2: For $u \in P$ and $r \geqslant 0$, we consider the ball $B_r(u)$ with its center at u and a radius of r w.r.t. the L_∞ metric. For the construction of G_2 we need the free space axes of the parameter cells and so called grid balls:

Definition 1 *Let $u \in P$ and $r \geqslant 0$ be chosen arbitrarily. The* grid ball $G_r(u)$ *is defined as the grid of $B_r(u)$ that has a mesh size of $\frac{\varepsilon}{456} w(u)$. We say $G_r(u)$* approximates *$B_r(u)$.*

We define G_2 as the monotone directed graph that is induced by the arrangement that is made up of the following components restricted to P:

- (1) All monotone free space axes restricted to their corresponding parameter cell.
- (2) All grid balls $G_{62w(u)}(u)$ for $u := \arg\min_{p \in e} w(u)$ and any parameter edge e.
- (3) The segments $\mathfrak{s}c_{\mathfrak{s}}$ and $\mathfrak{t}c_{\mathfrak{t}}$ if the parameter cells $C_{\mathfrak{s}}$ and $C_{\mathfrak{t}}$ that contain $\mathfrak{s}$ and $\mathfrak{t}$ are intersected by their corresponding monotone free space axes $\ell_{\mathfrak{s}}$ and $\ell_{\mathfrak{t}}$, where $c_{\mathfrak{s}}$ and $c_{\mathfrak{t}}$ are defined as the bottom-leftmost and top-rightmost point of $\ell_{\mathfrak{s}} \cap C_{\mathfrak{s}}$ and $\ell_{\mathfrak{t}} \cap C_{\mathfrak{t}}$.

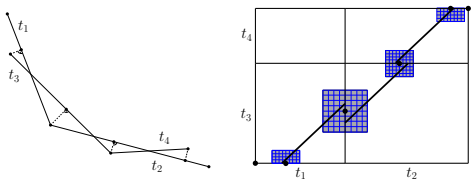

Exemplified construction of G_2 for two given polygonal curves T_1 and T_2. For simplicity we only illustrate four grid balls (with reduced radii) and the corresponding point pairs from $T_1 \times T_2$.

Finally, we set $w_2((v_1, v_2)) := |v_1 v_2|_w$ for all $(v_1, v_2) \in E_2$. For each edge $e \in G$ we choose the point $u \in e$ as the center of the corresponding grid ball because the free space axes of the parameters cells adjacent to e lie close to u.

Analysis of our approach: Since G_1 is monotone and each edge $(p_1, p_2) \in E_1$ is assigned to $|p_1 p_2|_w$, we obtain that for each path $\widetilde{\pi} \subset G_1$ between $\mathfrak{s}$ and $\mathfrak{t}$ holds $|\pi|_w \leqslant |\widetilde{\pi}|_w$. The same argument applies to G_2. Hence, we still have to ensure that there is a path $\widetilde{\pi} \subset G_1$ or $\widetilde{\pi} \subset G_2$ such that $|\widetilde{\pi}|_w \leqslant (1+\varepsilon)|\pi|_w$. We say that a path $\pi \subset P$ is *low* if $w(p) \leqslant \frac{\mu}{100}$ holds for all $p \in \pi$. For our analysis, we show the following:
Case A: There is a $\widetilde{\pi} \subset G_1$ with $|\widetilde{\pi}|_w \leqslant (1+\varepsilon)|\pi|_w$ if there is a shortest path $\pi \subset P$ that is not low (see Subsection 3.1).
Case B: Otherwise, there is a $\widetilde{\pi} \subset G_2$ with $|\widetilde{\pi}|_w \leqslant (1+\varepsilon)|\pi|_w$ (see Subsection 3.2).

3.1 Analysis of Case A

In this subsection, we assume that there is a shortest path π between $\mathfrak{s}$ and $\mathfrak{t}$ that is not low, i.e., there is a $p \in \pi$ with $w(p) \geqslant \frac{\mu}{100}$. Furthermore, for any $o, p \in \pi$, we denote the subpath of π which is between o and p by π_{op}. First we prove a lower bound for $|\pi|_w$ (Lemma 2). This lower bound ensures that the approximation error that we make for a path in G_1 is upper-bounded by $\varepsilon|\pi|_w$ (Lemma 3).

A *cell* C *of* G_1 is the convex hull of four vertices $v_1, v_2, v_3, v_4 \in V_1$ such that $C \cap V_1 = \{v_1, v_2, v_3, v_4\}$. As the mesh size of G_1 is $\frac{\varepsilon\mu}{40000(|T_1|+|T_2|)}$, we have $d_1(p_1, p_2) \leqslant \frac{\varepsilon\mu}{20000(|T_1|+|T_2|)}$ for any two points p_1 and p_2 that lie in the same cell of G_1. The following property of $w(\cdot)$ is the key in the analysis of the weighted shortest path length of G_1:

Definition 2 ([15]) *$f : P \to \mathbb{R}_{\geqslant 0}$ is 1-Lipschitz if $f(x) \leqslant f(y) + d_1(x, y)$ for all $x, y \in P$* [1].

Lemma 1 *$w(\cdot)$ is 1-Lipschitz w.r.t. L_1.*

Proof: Let $(a_1, a_2), (b_1, b_2) \in P$ be chosen arbitrarily. The subcurves $t_{T_1(a_1)T_2(b_2)} \subset T_1$ between $T_1(a_1)$ and $T_2(b_2)$ and $t_{T_2(a_2)T_2(b_2)} \subset T_2$ between $T_2(a_2)$ and $T_2(b_2)$ have lengths no larger than $|a_1 - b_2|$ and $|a_2 - b_2|$. Thus $d_2(T_1(a_1), T_1(b_1)) \leqslant |a_1 - b_1|$ and $d_2(T_2(a_2), T_2(b_2)) \leqslant |a_2 - b_2|$. Furthermore, $w((a_1, a_2))$ is equal to $d_2(T_1(a_1), T_2(a_2))$. By triangle inequality, $w((b_1, b_2)) = d_2(T_1(b_1), T_2(b_2)) \leqslant$

[1] The requirement $|f(x) - f(y)| \leqslant d_1(x, y)$ is also occasionally used to define 1-Lipschitz continuity. Note that this alternative definition is equivalent to Definition 2.

$d_2(T_2(b_2), T_2(a_2)) + d_2(T_2(a_2), T_1(a_1)) + d_2(T_1(a_1), T_1(b_1)) \leqslant d_1((a_1, a_2), (b_1, b_2)) + w((a_1, a_2))$, because $d_2(T_2(b_2), T_2(a_2)) = |b_2 - a_2|$, $d_2(T_2(a_2), T_1(a_1)) = w((a_1, a_2))$, $d_2(T_1(a_1), T_1(b_1)) = |b_1 - a_1|$, and $d_1((a_1, a_2), (b_1, b_2)) = |b_1 - a_1| + |b_2 - a_2|$. □

Lemma 1 allows us to prove the following lower bound for the weighted length of π.

Lemma 2 $|\pi|_w \geqslant \frac{\mu}{20000}$

Proof: Let $p \in \pi$ such that $w(p) \geqslant \frac{\mu}{100}$. Let $\psi := \pi \cap B_{\frac{\mu}{100}}(p)$. We have $|\psi|_w \geqslant \frac{\mu}{200}$ because $w(\cdot)$ is 1-Lipschitz. Furthermore, $\psi \subset \pi$ implies $|\psi|_w \leqslant |\pi|_w$ which yields $\frac{\mu}{200} \leqslant |\pi|_w$. □

Lemma 3 *There is a path $\widetilde{\pi} \subset G_1$ that connects $\mathfrak{s}$ and $\mathfrak{t}$ such that $|\widetilde{\pi}|_w \leqslant (1+\varepsilon)|\pi|_w$.*

Proof: Starting from $\mathfrak{s}$, we construct $\widetilde{\pi}$ inductively as follows: If π crosses a vertical (horizontal) parameter line next, $\widetilde{\pi}$ goes one step to the right (top). For $p \in \pi$ let h_p be the line with gradient -1 such that $p \in h_p$ (see the figure on the right). As π and $\widetilde{\pi}$ are monotone, $\widetilde{p} := h_p \cap \widetilde{p}$ is unique and well defined. For all p, p and $\widetilde{p}$ lie in the same cell of G_1 and thus, $w(\widetilde{p}) \leqslant w(p) + \frac{\varepsilon\mu}{20000(|T_1|+|T_2|)}$. This implies $|\widetilde{\pi}|_w \leqslant (1+\varepsilon)|\pi|_w$ because $|\widetilde{\pi}| = |\pi|$. To be more precise, we consider $\widetilde{\pi}, \pi : [0,1] \to P$ to be parametrized such that $d_1(\mathfrak{s}, \widetilde{\pi}(t)) = d_1(\mathfrak{s}, \widetilde{\pi}(t)) = t d_1(\mathfrak{s}, \mathfrak{t})$. We obtain, $||(\widetilde{\pi})'(t)||_1 = d_1(\mathfrak{s}, \mathfrak{t}) = ||(\pi)'(t)||_1$ for all $t \in [0,1]$.
Furthermore, the above implies $w(\widetilde{\pi}(t)) \leqslant w(\pi(t)) + \frac{\varepsilon\mu}{20000(|T_1|+|T_2|)}$ $(\star)$. Thus:

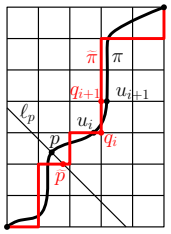

$$
\begin{aligned}
|\widetilde{\pi}|_w &= \int_0^1 w(\widetilde{\pi}(t))||(\widetilde{\pi})'(t)||_1 \, dt \overset{(\star)}{\leqslant} \int_0^1 \left(w(\pi(t)) + \frac{\varepsilon\mu}{20000(|T_1|+|T_2|)} \right) ||(\pi)'(t)||_1 \, dt \\
&= \int_0^1 w(\pi(t))||(\pi)'(t)||_1 \, dt + \frac{\varepsilon\mu \int_0^1 1 \; ||(\pi)'(t)||_1 \, dt}{20000(|T_1|+|T_2|)} \\
&= |\pi|_w + \frac{\varepsilon\mu}{20000} \overset{\text{Lemma 2}}{\leqslant} |\pi|_w + \varepsilon|\pi|_w = (1+\varepsilon)|\pi|_w.
\end{aligned}
$$

□

3.2 Analysis of Case B

In this subsection, we assume that there is a monotone low path π between $\mathfrak{s}$ and $\mathfrak{t}$. First, we make a key observation that is also of independent interest. It states that a shortest path (that is not necessarily low) inside a parameter cell is uniquely determined by its monotone free space axis.

Lemma 4 *Let C be an arbitrarily chosen parameter cell and $a, b \in C$ such that $a \leqslant_{xy} b$. Furthermore, let ℓ be the monotone free space axis of C and R the rectangle that is induced by a and b. The shortest path $\pi_{ab} \subset C$ between a and b is given as:*

- *$ac_1 \cup c_1c_2 \cup c_2b$, if ℓ intersects R in c_1 and c_2 such that $c_1 <_{xy} c_2$ and as*
- *$ac \cup cb$, otherwise, where c is defined as the closest point from R to ℓ.*

Proof: Let $\psi_{ab} \subset C$ by an arbitrary monotone path that connects a and b. In the following, we show that $|\pi_{ab}|_w \leqslant |\psi_{ab}|_w$. For this, we prove the following: Let $p \in C$ be chosen arbitrarily and q be its orthogonal projection onto ℓ (see Figure 4(b)). We show $w(r) \leqslant w(p)$ for $r \in pq$. This implies that there is an injective, continuous function $\perp : \psi_{ab} \to \pi_{ab}$ with $w(\perp(p)) \leqslant w(p)$ for all $p \in \psi$. In

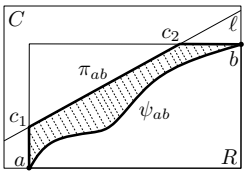

(a) Construction of a curve π_{ab} between a and b which is not longer than ψ_{ab}.

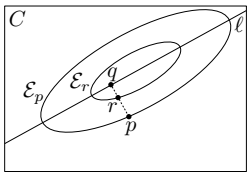

(b) Projecting a point orthogonally onto a free space axis reduces its weight.

Figure 4: A shortest weighted xy-monotone path between two points a and b with $a \leqslant_{xy} b$.

particular, $\perp(p)$ is defined as the intersection point of π_{ab} and the line d that lies perpendicular to ℓ such that $p \in d$. The function $\perp(\cdot)$ is well defined and injective as both ψ_{ab} and π_{ab} are monotone paths that connect a and b. Similarly, as in the proof of Lemma 3, this implies $|\pi_{ab}|_w \leqslant |\psi_{ab}|_w$ because $|\pi_{ab}| = |\psi_{ab}|$.

To be more precise, consider $\psi, \pi : [0,1] \to C$ to be parametrized such that $d_1(a, \psi(t)) = d_1(a, \pi(t)) = td_1(a,b)$. This implies $||(\psi)'(t)||_1 = d_1(a,b) = ||(\pi)'(t)||_1$ for all $t \in [0,1]$. Thus:

$$\begin{aligned} |\psi_{ab}|_w &= \int_0^1 w(\psi_{ab}(t))||(\psi_{ab})'(t)||_1 \, dt \geqslant \int_0^1 w(\perp(\psi_{ab}(t)))||(\pi_{ab})'(t)||_1 \, dt \\ &= \int_0^1 w(\pi_{ab}(t))||(\pi_{ab})'(t)||_1 \, dt = |\pi_{ab}|_w. \end{aligned}$$

Finally, we show: $w(r) \leqslant w(p)$, for $r \in pq$. Note that $w(r)$ and $w(p)$ are the leash lengths for r and p that lie on the boundary of the white space inside C, i.e., on the boundary of the ellipses $\mathcal{E}_r$ and $\mathcal{E}_p$, resp. (see Figure 4). Since $r \in pq$ we get $\mathcal{E}_r \subseteq \mathcal{E}_p$, which implies $w(r) \leqslant w(p)$. □

We call a point $p \in C$ *canonical* if $p \in \ell$. Let C_o and C_p be two parameter cells that share a parameter edge e. Furthermore, let $o \in \ell_0 \subset C_o$ and $p \in \ell_p \subset C_p$ be two canonical parameter points such that $o \leqslant_{xy} p$ where ℓ_o and ℓ_p are the monotone free space axis of C_o and C_p, respectively. Let c_o be the top-right end point of ℓ_o and c_p the bottom-left end point of ℓ_p. The following lemma is based on Lemma 4 and characterizes how a shortest path passes through the parameter edges.

Lemma 5 *If $c_o, c_p \in e$ and $c_o \leqslant_{xy} c_p$, π_{op} is equal to the concatenation of the segments oc_o, c_oc_p, and c_pp (see figure (a) on right). Otherwise, there is a $z \in e$ such that π_{op} is equal to the concatenation of the segments oz_o, z_oz_p, and z_pp, where $z_o \in \ell_{C_o}$ and $z_p \in C_p$ such that z is the orthogonal projection of z_o and z_p onto e (see figure (b)).*

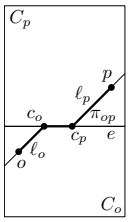

(a) π_{op} for $o \leqslant_{xy} p$

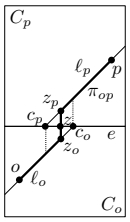

(b) π_{op} for $o \not\leqslant_{xy} p$

Outline of the analysis of Case B: In the following, we apply Lemmas 4 and 5 to subpaths π_{ab} of π in order to ensure that π_{ab} is a subset of the union of a constant number of balls (that are approximated by grid balls in our approach) and monotone free space axes. In particular, we construct a discrete sequence of points from π which lie on the free space axes, see Subsection 3.2.1. For each induced subpath π_{ab}, we ensure that π_{ab} crosses one or two perpendicular parameter edges. For the analysis we distinguish between the two cases which we consider separately:
Case 1: π_{ab} crosses one parameter edge and **Case 2:** π_{ab} crosses two parameter edges.

For Case 1, we show that, if π_{ab} crosses one edge (e) then π_{ab} is a subset of the union of the two monotone free space axes of the parameter cells that share e and the ball $B_{62w(u)}(u)$ for

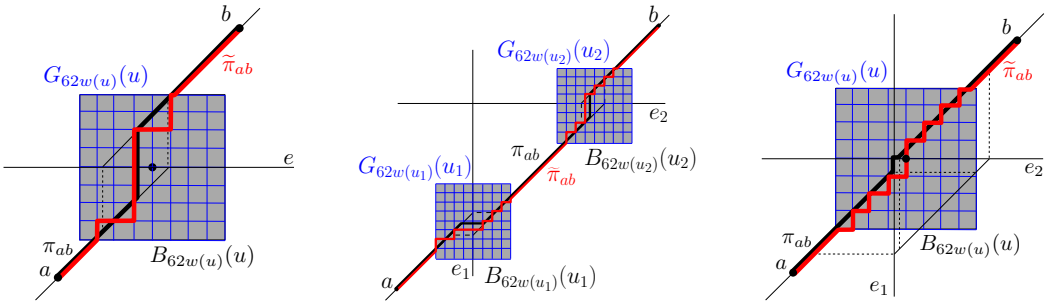

(a) Case (1.) (b) Case (2.1.) (c) Case (2.2.)

Figure 5: Three different subcases in which we ensure, differently, that we capture a subpath $\pi_{ab} \subset \pi$ by balls and free space axes. Path π_{ab} is approximated by a path $\widetilde{\pi}_{ab}$ in the graph that is induced by these free space axis and the corresponding grid balls.

$u := \arg\min_{p \in e} w(u)$ (see Figure 5(a) and Subsections 3.2.2).

For Case 2, (see Subsection 3.2.3), we consider the case that π_{ab} crosses two parameter edges e_1 and e_2. In particular, π_{ab} runs through three parameter cells C_q, C_r, and C_s, where C_q and C_r share e_1 and C_r and C_s share e_2.

We further distinguish further between two subcases. For this, let $u_1 := \arg\min_{p \in e_1} w(p)$ and $u_2 := \arg\min_{p \in e_2} w(p)$.

Case 2.1: We show that, if $d_1(u_1, u_2) \geqslant 6 \max\{w(u_1), w(u_2)\}$, then π_{ab} is a subset of the union of the balls $B_{62w(u_1)}(u_1)$ and $B_{62w(u_2)}(u_2)$ and the monotone free space axes of C_q, C_r, and C_s (see Figure 5(b) and Lemma 9).

Case 2.2: We show that, if $d_1(u_1, u_2) \leqslant 6 \max\{w(u_1), w(u_2)\}$, then π_{ab} is a subset of the union of the ball $B_{62w(u)(u)}$ and the monotone free space axes of C_q and C_s (see Figure 5(c) and Lemma 13).

For the analysis of the length of a shortest path $\widetilde{\pi} \subset G_2$ that lies between $\mathfrak{s}$ and $\mathfrak{t}$, we construct for $\pi_{ab} \subset \pi$ a path $\widetilde{\pi}_{ab} \subset G_2$ between a and b such that $|\widetilde{\pi}_{ab}|_w \leqslant (1+\varepsilon)|\pi_{ab}|_w$. In particular, $\widetilde{\pi}_{ab}$ is a subset of the grid balls that approximate the above considered balls and the free space axes that are involved in the individual (sub-)case for π_{ab} (see, Figure 5). Finally, we define $\widetilde{\pi} \subset G_2$ as the concatenation of the approximations $\widetilde{\pi}_{ab}$ for all π_{ab}.

3.2.1 Separation of a shortest path

In the following, we determine a discrete sequence of canonical points $\mathfrak{s} = p_1, ..., p_k = \mathfrak{t} \in \pi$ such that $\pi_{p_i p_{i+1}}$ crosses at most two parameter lines for each $i \in \{1, ..., k-1\}$. First we need the following supporting lemma:

Lemma 6 *For all $q_1, q_2 \in \pi$ that lie in the same parameter cell with $q_1 \leqslant_{xy} q_2$ we have $q_2.y - q_1.y - \frac{\mu}{50} \leqslant q_2.x - q_1.x \leqslant q_2.y - q_1.y + \frac{\mu}{50}$.*

Proof: The triangle inequality implies:
$d_2(T_2(q_2.y), T_2(q_1.y)) \leqslant d_2(T_2(q_2.y), T_1(q_2.x)) + d_2(T_1(q_2.x), T_1(q_1.x)) + d_2(T_1(q_1.x), T_2(q_1.y))$. This implies $d_2(T_2(q_2.y), T_2(q_1.y)) - \frac{\mu}{50} \leqslant d_2(T_1(q_2.x), T_1(q_1.x))$, because
$d_2(T_2(q_2.y), T_1(q_2.x)), d_2(T_1(q_1.x), T_2(q_1.x)) \leqslant \frac{\mu}{100}$. Furthermore, $d_2(T_2(q_2.y), T_2(q_1.y)) = q_2.y - q_1.y$ and $d_2(T_1(q_2.x), T_1(q_1.x)) = q_2.x - q_1.x$ because q_1 and q_2 lie in the same cell. This implies $q_2.y - q_1.y - \frac{\mu}{50} \leqslant q_2.x - q_1.x$. A corresponding argument yields $q_2.x - q_1.x \leqslant q_2.y - q_1.y + \frac{\mu}{50}$. □

Lemma 7 *There are canonical points $\mathfrak{s} = p_1, \dots p_k = \mathfrak{t} \in \pi$ such that for all $i \in \{1, \dots, k-1\}$ the following holds: (P1) $\pi_{p_i p_{i+1}}$ crosses at most one vertical and at most one horizontal parameter line which are both not part of ∂P and (P2) the distance of p_i to a parameter line is lower-bounded by $\frac{\mu}{6}$ for all $i \in \{2, \dots, k-1\}$.*

Proof: First, we give the construction of $p_2, \dots, p_{k-1}$. After that, we establish Properties (P1) and (P2), for each $i \in \{1, \dots, k-1\}$.

- Construction of $p_2, \dots, p_{k-1}$: We construct $p_2, \dots, p_{k-1}$ iteratively with $p_1 := \mathfrak{s}$. Point p_2 is defined as the first point on π such that $p.x = \frac{\mu}{2}$ or $p.y = \frac{\mu}{2}$. For $i \in \{2, \dots, k-3\}$, let $p_1, \dots, p_i$ be defined, c be the top-right corner of the parameter cell that contains p_i, and u_1 be the next intersection point of π (behind p_i) with the parameter grid, see Figure 6. W.l.o.g., we assume that u_1 lies on a vertical parameter line.

  If $d_1(c, u_1) \geqslant \frac{\mu}{2}$, we define p_{i+1} as the first point on π with $p_{i+1}.y = u_1.y + \frac{c.y - u_1.y}{2}$ or $p_{i+1}.x = u_1.x + \frac{\mu}{4}$, see Figure 6(a).

  If $d_1(c, u_1) < \frac{\mu}{2}$, we consider the next intersection point u_2 of π with a horizontal parameter line such that $u_1 \leqslant_{xy} u_2$. We define p_{i+1} as the first point behind u_2 such that $p_{i+1}.y = u_2.y + \frac{\mu}{4}$.

(a) Construction of p_{i+1} for $d_1(u_1, c) \geqslant \frac{\mu}{2}$. (b) Construction of p_{i+1} for $d_1(u_1, c) < \frac{\mu}{2}$.

Figure 6: The iterative construction of p_{i+1} distinguishes between the two cases depending on whether the next intersection u_1 of π and the parameter grid lies close to a vertex c of the parameter grid or not.

- (P1) and (P2): W.l.o.g., we assume $u.x = c.x$. For the configurations of $u.y = c.y$ a symmetric argument applies. Assume p_{i-1} and $\pi_{p_{i-1} p_i}$ fulfil (P1) and (P2) for $i \in \{2, \dots, k-2\}$. We show that p_i fulfils (P1) and $\pi_{i_i i_{i+1}}$ (P2) for the two cases $d_1(c, u_1) \geqslant \frac{\mu}{2}$ and $d_1(c, u_1) < \frac{\mu}{2}$ separately. By induction it follows the statement of the lemma.
  - $d_1(c, u_1) \geqslant \frac{\mu}{2}$:
    - (P1): In both subcases $p_{i+1}.y = u_1.y + \frac{c.y - u_1.y}{2}$ or $p_{i+1}.x = u_1.x + \frac{\mu}{4}$ it follows that p_{i+1} lies in the parameter cell C_r that lies to the right of the parameter cell that contains p_1. In particular, in the first (second) subcase p_{i+1} lies by construction in the same parameter row (column). As π is monotone and p_{i+1} is defined as the first point that fulfils one of the two constraints, $p_{i+1} \in C_r$. This implies (P1).
    - (P2): The above argument implies that the distances of p_{i+1} to the right and the top parameter line are lower-bounded by $\frac{\mu}{2}$. If $p_{i+1}.y = u_1.y + \frac{c.y - u_1.y}{2}$, we have $p_{i+1}.y - u_1.y = \frac{c.y - u_1.y}{2} \geqslant \frac{\mu}{4}$. Thus, Lemma 6 implies $p_{i+1}.x - u_1.x \geqslant \frac{\mu}{4} - \frac{\mu}{50} \geqslant \frac{\mu}{6}$ which yields that the distance of p_{i+1} to the left parameter line is lower-bounded

by $\frac{\mu}{6}$. If $p_{i+1}.x = u_1.x + \frac{\mu}{4}$, we have $p_{i+1}.x - u_1.x = \frac{\mu}{4}$. Thus, Lemma 6 implies $p_{i+1}.y - u_1.y \geqslant \frac{\mu}{4} - \frac{\mu}{50} \geqslant \frac{\mu}{6}$ which yields that the distance of p_{i+1} to the bottom parameter line is lower-bounded by $\frac{\mu}{6}$. Hence, (P2) is fulfilled.

– $d_1(c, u_1) < \frac{\mu}{2}$:
  * (P1): Assume π crosses another vertical parameter line in a point u that lies before u_2. This implies, $u.x - u_1.x \geqslant \mu$ and $u.y - u_1.y \leqslant \frac{\mu}{2}$. Hence, $u.x - u_1.x \geqslant 2(u.y - u_1.y)$ which is a contradiction to Lemma 6. Thus, (P1) is fulfilled.
  * (P2): The construction of u_2 implies that the distances to the bottom and to the top parameter line is lower-bounded by $\frac{\mu}{4}, \frac{3\mu}{4} \geqslant \frac{\mu}{6}$. Finally, we lower-bound the distances of p_{i+1} to the left and to the right parameter line as follows: By combining $u_2.y - u_1.y \leqslant \frac{\mu}{2}$ and Lemma 6 we obtain $c.x \leqslant u_2.x \leqslant c.x + \frac{\mu}{2} + \frac{\mu}{50}$. Another application of Lemma 6, combined with $p_{i+1}.y = u_2.y + \frac{\mu}{4}$ leads to $c.x + \frac{\mu}{4} - \frac{\mu}{50} \leqslant p_{i+1}.x \leqslant c.x + \frac{\mu}{2} + \frac{\mu}{50} + \frac{\mu}{4} + \frac{\mu}{50}$. Thus, the distances of p_{i+1} to the left and to the right parameter line are lower-bounded by $\frac{\mu}{6}$. Hence, (P2) is fulfilled.

□

3.2.2 Analysis of subpaths that cross one parameter edge

We need to show that those parts of π that do not lie on the free space axes are covered by the balls $B_{62w(u)}$. For this, we use the following geometrical interpretation of the free space axes ℓ and $\hbar$ of a parameter cell C. Let $t_1 \in T_1$ and $t_2 \in T_2$ be the segments that correspond to C. We denote the angular bisectors of t_1 and t_2 by d_ℓ and $d_\hbar$ such that the start points $t_1(0)$ and $t_2(0)$ of t_1 and t_2 lie on different sides w.r.t. ℓ, see Figure 7(b). If t_1 and t_2 are parallel, d_ℓ denotes the line between t_1 and t_2 and we declare $d_\hbar$ as undefined[2]. We observe (see Figure 7):

Observation 2 *$q \in \ell \Leftrightarrow T_1(q.x)T_2(q.y) \perp d_\ell$ and $p \in \hbar \Leftrightarrow T_1(p.x)T_2(p.y) \perp d_\hbar$.*

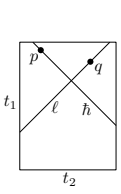

(a) Point $p \in \ell$ and $q \in \hbar$.

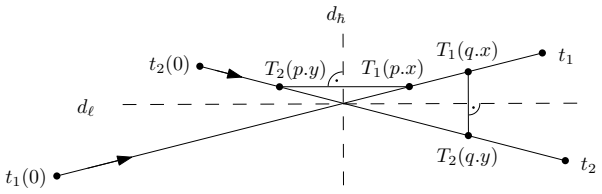

(b) To p and q corresponding leashes.

Figure 7: Duality of parameter points from ℓ ($\hbar$) and leashes that lie perpendicular to d_ℓ ($d_\hbar$).

From now on, let $o, p \in \pi$ be two consecutive, canonical points that are given via Lemma 7 such that $o \leqslant_{xy} p$. Furthermore, let ℓ_o and ℓ_p be the free space axes of the parameter cells C_o and C_p such that $o \in \ell_o \subset C_o$ and $p \in \ell_p \subset C_p$.

Lemma 8 *If π_{op} crosses one parameter edge e, $c_o, c_p \in e$ exist and we have $d_\infty(c_0, c_p) \leqslant \frac{w(u)}{2}$ where $u = \arg\min_{p \in e} w(p)$.*

[2]There is a corresponding definition of $\hbar$ in the case of $t_1 \parallel t_2$. However, considering $\hbar$ for $t_1 \parallel t_2$ would unnecessarily complicate the presentation because $\hbar$ is not required.

Proof: W.l.o.g., we assume that e is horizontal. Let $t_1, t_2 \in T_1$ and $t_3 \in T_2$ be the segments that induce parameter cells C_o and C_p. First, we show $\angle(t_1, t_3), \angle(t_2, t_3) \leqslant 7^\circ$ and, then, that $d_1(c_0, c_p) \leqslant w(u)$. Let $q_1 \in \ell_o$ and $q_2 \in \ell_p$ such that $q_1.x = c_p$ and $q_2.x = c_o$, see Figure 8(a). $\angle(t_1, t_3) \leqslant 7^\circ$ implies $\angle(T_1(u.x)T_2(u.y), T_1(u.x)T_2(q_2.y)) \leqslant 3.5^\circ$. Furthermore, $c_p = e \cap \ell_p$ implies: c_p corresponds to a leash $l_p = (T_1(c_p.x), T_2(c_p.y))$ such that $T_1(c_p.x) = T_1(u.x)$ and $T_1(c_p.x), T_2(c_p.y) \perp d_{\ell_o}$, see Figure 8(b). Thus, $d_2(T_2(q_2.y), T_2(u.y))$ is upper-bounded by $d_2(T_2(u.y), T_2(q_2.y))$ which is upper-bounded by $d_2(T_1(u.x), T_2(u.y)) \tan(3.5^\circ) \leqslant 0.065 w(u) < \frac{w(u)}{2}$.

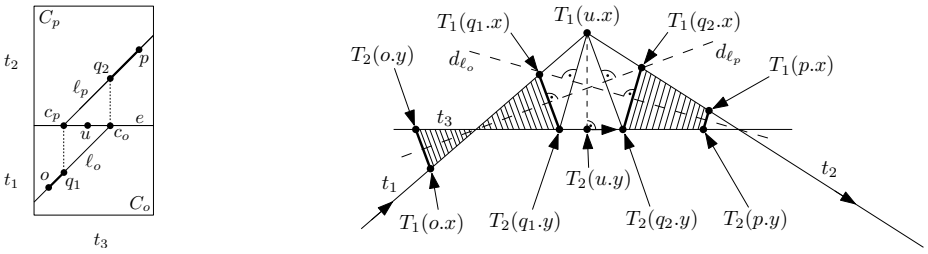

(a) The subpath $\pi_{op} \backslash (\ell \cup \hbar)$ lies in the convex hull of q_1, c_o, q_2, and c_p.

(b) The length of the subcurve of T_1 that corresponds to the x-coordinates of the points from $\pi_{op} \backslash (\ell \cup \hbar)$ depends on $d_2(T_1(u.x), T_2(u.y))$.

Figure 8: Configuration of the Lemmas 8 and 9: The length of the subpath of π_{op} that does not necessarily lie on $\ell \cup \hbar$ is related to $w(u)$.

Finally, we show $\angle(t_1, t_3), \angle(t_2, t_3) \leqslant 7^\circ$: We have $d_2(T_1(o.x), T_2(o.y)), d_2(T_1(u.x), T_2(u.x)) \leqslant \frac{\mu}{100}$ because π is low. Lemma 7 implies $d_2(T_1(o.x), T_1(u.x)), d_2(T_2(o.y), T_2(u.y)) \geqslant \frac{\mu}{6}$. Thus, $\angle(t_1, t_3) \leqslant \arcsin \frac{6}{50} \leqslant 7^\circ$. A similar argument implies that $\angle(t_2, t_3) \leqslant \arcsin \frac{6}{50} \leqslant 7^\circ$ □

Lemma 9 *$\pi_{op} \subset \ell_o \cup B_{w(u)}(u) \cup \ell_p$ (see Figure 5(a)).*

Proof: We combine Lemmas 5 and 8. Lemma 5 implies that π_{op} orthogonally crosses e at a point z that lies between c_o and c_p such that $z \in z_o z_p \subset \pi_{op}$. Lemma 8 implies $d_1(c_o, c_p) \leqslant \frac{w(u)}{2}$. Thus, $z_o z_p \subset B_{w(u)}(u)$. Furthermore, $o z_o \subset \ell_o$ and $z_p p \subset \ell_p$. This implies $\pi_{op} \subset \ell_o \cup B_{w(u)}(u) \cup \ell_p$ because $\pi_{op} = o z_o \cup z_o z_p \cup z_p p$. □

Lemma 10 *There is a path $\widetilde{\pi}_{op} \subset G_2$ between o and p such that $|\widetilde{\pi}_{op}|_w \leqslant (1+\varepsilon)|\pi_{op}|_w$.*

Proof:: By Lemma 9, the two following intersection points are well defined: Let z_o be the intersection point of ℓ_o and $\partial B_{62w(u)}(u)$ which lies on the left or bottom edge of $\partial B_{62w(u)}(u)$. Analogously, let z_p be the intersection point of ℓ_p and $\partial B_{62w(u)}(u)$ which lies on the right or top edge of $\partial B_{62w(u)}(u)$. By Lemma 9, we can subdivide π_{op} into the three pieces $o z_o \subset \ell_o$, $\pi_{z_o z_p}$, and $z_p p \subset \ell$. As $o z_o, z_p p \subset G_2$, we just have to construct a path $\widetilde{\pi}_{z_o z_p} \subset G_2$ between z_o and z_p such that $|\pi_{z_o z_p}|_w \leqslant (1+\varepsilon)|\widetilde{\pi}_{z_o z_p}|_w$.

We construct $\widetilde{\pi}_{z_o z_p}$ by applying the same approach as used in the proof of Lemma 3, see Figure 5(a).

To upper-bound $|\widetilde{\pi}_{z_o z_p}|_w$ by $(1+\varepsilon)|\pi_{z_o z_p}|_w$ we first lower-bound $|\pi_{z_o z_p}|_w$ by $\frac{1}{2}w^2(u)$. Then, we apply an approach that is similar to the approach used in the proof of Lemma 3

- $|\pi_{z_o z_p}|_w \geqslant \frac{1}{2}w^2(u)$: Let $\psi := \pi_{z_o z_p} \cap B_{w(u)}(u)$. As $|\psi| \geqslant w(u)$ and $w(\cdot)$ is 1-Lipschitz, we obtain $|\psi|_w \geqslant \frac{1}{2}w^2(u)$. This implies $|\pi_{z_o z_p}|_w \geqslant \frac{1}{2}w^2(u)$ because $\psi \subset \pi_{z_o z_p}$.

- $|\widetilde{\pi}_{z_o z_p}|_w \leqslant (1+\varepsilon)|\pi_{z_o z_p}|_w$: We observe that $|\pi_{z_o z_p}| \leqslant 114w(u)$ ($\ddagger$) because $\pi_{z_o z_p}$ is monotone and $\pi_{z_o z_p} \subset B_{62w(u)}(u)$. Furthermore, we parametrize $\widetilde{\pi}_{z_o z_p}, \pi_{z_o z_p} : [0,1] \to P$ such that $d_1(z_o, \widetilde{\pi}_{z_o z_p}) = d_1(z_o, \pi_{z_o z_p})$. This implies $w(\widetilde{\pi}_{z_o z_p}(t)) \leqslant w(\pi_{z_o z_p}(t)) + \frac{\varepsilon w(u)}{228}$ ($\dagger$) and $||(\widetilde{\pi}_{z_o z_p})'(t)||_1 = ||(\pi_{z_o z_p})'(t)||_1$ ($\star$) for all $t \in [0,1]$. Thus:

$$
\begin{aligned}
|\widetilde{\pi}_{z_o z_p}|_w &= \int_0^1 w(\widetilde{\pi}_{z_o z_p}(t))||(\widetilde{\pi}_{z_o z_p})'(t)||_1 \, dt \\
&\overset{(\dagger)+(\star)}{\leqslant} \int_0^1 w(\pi_{z_o z_p})||(\pi_{z_o z_p})'(t)||_1 \, dt + \frac{\varepsilon w(u)}{228} \int_0^1 ||(\pi_{z_o z_p})'(t)||_1 \, dt \\
&\overset{(\ddagger)}{\leqslant} |\pi_{z_o z_p}|_w + \frac{\varepsilon}{2} w^2(u) \\
&\overset{|\pi_{z_o z_p}|_w \geqslant \frac{1}{2}w^2(u)}{\leqslant} (1+\varepsilon)|\pi_{z_o z_p}|_w.
\end{aligned}
$$

□

3.2.3 Analysis of subpaths that cross two parameter edges

Let q and s be two consecutive parameter points from $\{p_2, \ldots, p_{k-1}\}$ such that π_{qs} crosses two parameter edges e_1 and e_2. By Lemma 7, e_1 and e_2 are perpendicular to each other and are adjacent at a point c. Let C_r be the parameter cell such that e_1 and e_2 are part of the boundary of C_r. Furthermore, let C_q and C_s be the parameter cells such that $q \in C_q$ and $s \in C_s$. We denote the monotone free space axis of C_q, C_r, and C_s by ℓ_q, ℓ_r, and ℓ_s, respectively. Let $u_1 := \arg\min_{a \in e_1} w(a)$ and $u_2 := \arg\min_{a \in e_2} w(a)$.

Lemma 11 *If $d_1(u_1, u_2) \geqslant 6\max\{w(u_1), w(u_2)\}$, there is another canonical parameter point $r \in \ell_r$ such that $\pi_{qs} \subset \ell_q \cup B_{w(u_1)}(u_1) \cup \ell_r \cup B_{w(u_2)}(u_2) \cup \ell_s$.*

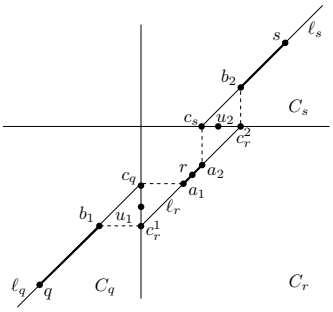

(a) Construction of π_{qs} s.t. $qb_1, a_1a_2, b_2w \subset \pi_{qs}$, $\pi_{b_1a_1} \subset B_{w(u_1)}(u_1)$, and $\pi_{a_1b_2} \subset B_{w(u_2)}(u_2)$

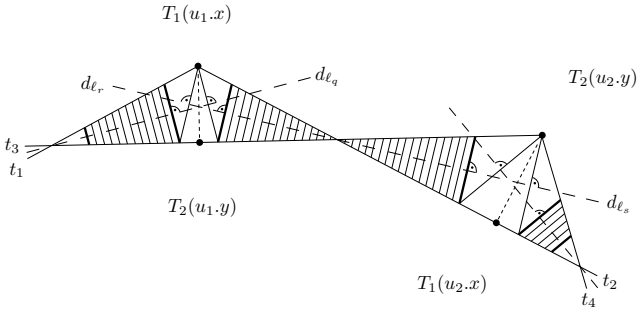

(b) The matching that corresponds π_{qs} has three parts in that the matched points from $T_1 \times T_2$ lie perpendicular to the corresponding angular bisector

Figure 9: Configuration of Lemma 11 in the Euclidean space of T_1 and T_2 and in the parameter space of π_{qs}: There are three supaths $qb_1, a_1a_2, b_2s \subset \pi_{qs}$ that lie on monotone free space axis ℓ_q, ℓ_r, and ℓ_s and, thus, three parts of the corresponding matching which are made up of leashes that are perpendicular to the diagonals d_{ℓ_q}, d_{ℓ_r}, and d_{ℓ_s} that correspond to ℓ_q, ℓ_r, and ℓ_s.

Proof: W.l.o.g., assume that π_{qs} crosses first a vertical parameter edge. Let $t_1, t_2 \in T_1$ and $t_3, t_4 \in T_2$ be the segments that induce parameter cells C_q, C_r, and C_s, see Figure 9. Let c_q and c_r^2 be the top-right end points of ℓ_q and ℓ_r, respectively. Let c_r^2 and c_s be the bottom-left end points of ℓ_r and ℓ_s, respectively (see Figure 9(a)). Let $a_1, a_2 \in \ell_r$ such that $c_q.y = a_1.y$ and $a_2.x = c_s.x$. Furthermore, let $b_1 \in \ell_q$ and $b_2 \in \ell_s$ such that $b_1.y = c_r^1$ and $c_r^2.x = b_2.x$. In the following, we show that $qb_1, a_1a_2, b_2s \subset \pi_{qs}$, $b_1, a_1 \in B_{w(u_1)}(u_1)$, and $b_2, a_2 \in B_{w(u_2)}(u_2)$. This implies $\pi_{qs} \subset \ell_q \cup B_{w(u_1)}(u_1) \cup \ell_r \cup B_{w(u_2)}(u_2) \cup \ell_s$ and concludes the proof.

Below, we show $\angle(t_2, t_3) \leqslant 42^\circ$. Then, a similar argument as used in Lemma 8 implies $d_1(c_r^1, u_1), d_1(c_q, u_1) \leqslant \frac{w(u_1)}{2}$ and $d_1(c_s, u_2), d_1(c_r^2, u_2) \leqslant \frac{w(u_1)}{2}$. Finally, we show $\angle(t_2, t_3) \leqslant 42^\circ$: $d_1(u_1, u_2) \geqslant 6\max\{w(u_1), w(u_2)\}$ implies that $d_2(T_1(u_1.x), T_2(u_1.y))$ and $d_2(T_1(u_2.x), T_2(u_2.y))$ are upper-bounded by $3\min\{d_2(T_1(u_1.x), T_1(u_2.x)), d_2(T_2(u_1.y), T_2(u_2.y))\}$. Thus, we obtain $\angle(t_2, t_3) \leqslant \arcsin(\frac{2}{3}) < 42^\circ$. □

Lemma 12 *If $d_1(u_1, u_2) \geqslant 6\max\{w(u_1), w(u_2)\}$, there is a path $\widetilde{\pi}_{qs} \subset G_2$ between q and s such that $|\widetilde{\pi}_{qs}|_w \leqslant (1+\varepsilon)|\pi_{oqs}|_w$.*

Proof: Lemma 11 implies that the following constructions are unique and well defined: Let z_1 (z_2) be the intersection point of $\partial B_{w(u_1)}(u_1)$ and ℓ_q (ℓ_r) that lies on the left or bottom (respectively, right or top) edge of $\partial B_{w(u_1)}(u_1)$. Analogously, let z_3 (z_4) be the intersection point of $\partial B_{w(u_2)}(u_2)$ and ℓ_r (ℓ_s) that lies on the left or bottom (respectively, right or top) edge of $\partial B_{w(u_2)}(u_2)$. By applying the approach of Lemma 10, for $\pi_{z_1z_2}$ and $\pi_{z_3z_4}$, we obtain a path $\widetilde{\pi}_{z_1z_2} \subset G_2$ between z_1 and z_2 and a path $\widetilde{\pi}_{z_3z_4} \subset G_2$ between z_3 and z_4 such that $|\widetilde{\pi}_{z_1z_2}|_w \leqslant (1+\varepsilon)|\pi_{z_1z_2}|_w$ and $|\widetilde{\pi}_{z_3z_4}|_w \leqslant (1+\varepsilon)|\pi_{z_3z_4}|_w$. This concludes the proof because $qz_1, z_2z_3, z_4s \subset G_2$. □

Lemma 13 *If $d_1(u_1, u_2) \leqslant 6\max\{w(u_1), w(u_2)\}$, we have $\pi_{qs} \subset \ell_q \cup B_{62w(u)}(u) \cup \ell_s$ where $u := \arg\max_{u \in \{u_1, u_2\}}\{w(u_1), w(u_2)\}$.*

Proof: Let $a \in \pi_{qs}$ be the last point that lies on ℓ_q, i.e., there is no point $d \in \pi \cap \ell_q \backslash \{a\}$ such that $a \leqslant_{xy} d$, see Figure 10(b). In the following, we show $d_1(a, c) \leqslant 56\max\{w(u_1), w(u_2)\}$. Analogously, we construct the first point $b \in \pi_{qs}$ that lies on ℓ_s, i.e., there is no point $d \in \pi \cap \ell_s \backslash \{b\}$, see Figure 10(b). A similar argument as above implies $d_1(b, c) \leqslant 56\max\{w(u_1), w(u_2)\}$. The triangle inequality implies $d_1(d, u) \leqslant d_1(d, c) + d_1(c, u) \leqslant 62\max\{w(u_1), w(u_2)\}$ for all $d \in \pi_{ab}$ and $u \in \{u_1, u_2\}$. This concludes the proof.

For the sake of contradiction we assume $d_1(a, c) \geqslant 56\max\{w(u_1), w(u_2)\}$. Lemma 4 implies that π_{ab} crosses the boundary ∂C_q of C_q in the orthogonal projection a_1 of a onto the top edge of ∂C_q or in the orthogonal projection a_2 of a onto the right edge of ∂C_q, see Figure 10(b). Thus, even $aa_1 \subset \pi_{qs}$ or $aa_2 \subset \pi_{ab}$ because π_{ab} is monotone. In the following, we show $|aa_1|_w, |aa_2|_w \geqslant 0.4874\lambda^2(\max\{w(u_1), w(u_2)\})^2$ where $\lambda \geqslant 0$ such that $d_1(u_1, a) = \lambda\max\{w(u_1), w(u_2)\}$. This implies $|\pi_{ab}|_w \geqslant 0.4874\lambda^2\max^2\{w(u_1), w(u_2)\}$.

Furthermore, we construct another path $\widetilde{\pi}_{ab}$ connecting a and b such that $|\widetilde{\pi}_{ab}|_w < (4\lambda(1.01 + 0.09\lambda) + 114)(\max\{w(u_1), w(u_2)\})^2$. Additionally, we show $\lambda \geqslant 50$. This is a contradiction to the fact that π_{ab} is a shortest path between a and b:

$$
\begin{aligned}
& |\pi_{ab}|_w && \leqslant |\widetilde{\pi}_{ab}|_w \\
\Rightarrow\ & 0.4874\lambda^2(\max\{w(u_1), w(u_2)\})^2 && \leqslant (4\lambda(1.01 + 0.09\lambda) + 114)(\max\{w(u_1), w(u_2)\})^2 \\
\Leftrightarrow\ & 0.4874\lambda^2 && \leqslant \lambda^2\left(\frac{4.04}{\lambda} + 0.36 + \frac{114}{\lambda^2}\right) \\
\overset{\lambda \geqslant 50}{\Rightarrow}\ & 0.4874 && \leqslant 0.0808 + 0.36 + 0.0456 = 0.4864
\end{aligned}
$$

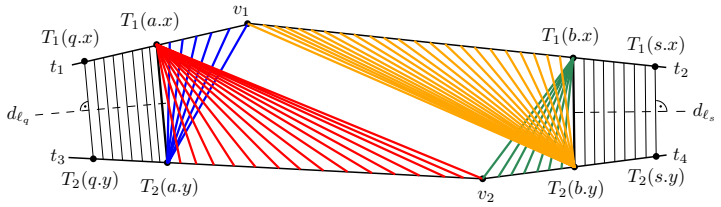

(a) The paths (1.) aa_1 (red), (2.) aa_2 (blue), (3.) bb_1 (green), and (4.) bb_2 (orange) correspond to matchings such the matched points (1.) on T_1 are just $T_1(a.x)$ (red), (2.) on T_2 are just $T_2(a.y)$ (blue), (3.) on T_1 are just $T_1(b.x)$ (green), and (4.) on T_2 are just $T_2(b.y)$ (orange)

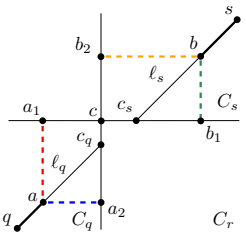

(b) Even π_{ab} crosses ∂C_q orthogonally in a_1 or in a_2 and ∂C_s orthogonally even in b_1 or in b_2.

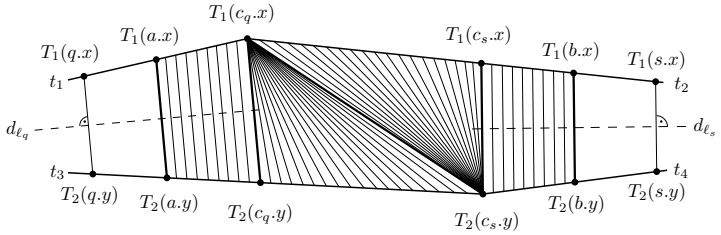

(c) Matching that corresponds to $\widetilde{\pi}_{ab}$

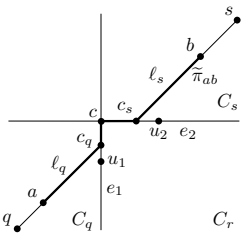

(d) Construction of $\widetilde{\pi}_{ab}$

Figure 10: Two paths $\widetilde{\pi}_{ab}$ and π_{ab} and the corresponding matchings: The shortest path π_{ab} that "leaves" ℓ_q at the point a and enters ℓ_q at the point b and the path $\widetilde{\pi}_{ab}$ that is constructed such that $ac_q, c_sb \subset \widetilde{\pi}_{ab}$.

- Construction of $\widetilde{\pi}_{ab}$: Let c_q be the top-right end point of ℓ_q and c_s the bottom-left end point of ℓ_s, see Figure 10(d). We define $\widetilde{\pi}_{qs} := ac_q \cup c_qc \cup cc_s \cup c_sb$.
- Upper bound for $|\widetilde{\pi}_{ab}|_w$: First of all we show $d_1(a, c_q) \leqslant 2\lambda \max\{w(u_1), w(u_2)\}$. After that we show $w(d) \leqslant (1.01 + 0.09\lambda) \max\{w(u_1), w(u_2)\}$ for all $d \in ac_q$. This implies $|\widetilde{\pi}_{ac_q}|_w \leqslant 2\lambda(1.01 + 0.09\lambda)(\max\{w(u_1), w(u_2)\})^2$. A similar argument implies $|\widetilde{\pi}_{c_sb}|_w \leqslant 2\lambda(1.01 + 0.09\lambda)(\max\{w(u_1), w(u_2)\})^2$. Furthermore, we show $d_1(c_q, c) \leqslant 7 \max\{w(u_1), w(u_2)\}$ and $w(d) \leqslant 8.01 \max\{w(u_1), w(u_2)\}$ for all $d \in c_qc$. This implies $|\widetilde{\pi}_{c_qc}|_2 \leqslant 57(\max\{w(u_1), w(u_2)\})^2$. A similar argument implies $|\widetilde{\pi}_{cc_s}|_w \leqslant 57(\max\{w(u_1), w(u_2)\})^2$. Finally we upper bound

$$\begin{aligned} |\widetilde{\pi}_{ab}|_w &= |\widetilde{\pi}_{ac_q}|_w + |\widetilde{\pi}_{c_qc}|_w + |\widetilde{\pi}_{cc_s}|_w + |\widetilde{\pi}_{c_sb}|_w \\ &\leqslant (4\lambda(1.01 + 0.09\lambda) + 114)(\max\{w(u_1), w(u_2)\})^2. \end{aligned}$$

  - $d_1(a, c_q) \leqslant 2\lambda \max\{w(u_1), w(u_2)\}$: $d_1(u_1, a) = \lambda \max\{w(u_1), w(u_2)\}$ implies $d_1(a, e_1) \leqslant \lambda \max\{w(u_1), w(u_2)\}$. As the gradient of ℓ_q is 1 and $c_q \in \ell_q$, we have $d_1(a, c_q) \leqslant 2\lambda \max\{w(u_1), w(u_2)\}$.
  - $w(d) \leqslant (1.01 + 0.09\lambda)w(u_1)$ for all $d \in ac_q$: First we show $\angle(t_1, t_3) \leqslant 10°$: By Lemma 7 we know $d_1(q, e_1) \geqslant \frac{\mu}{6}$. Let $d := \pi_{ab} \cap e_1$. This implies $d_1(q, d) \geqslant \frac{\mu}{2}$. Furthermore, we have $w(q), w(d) \leqslant \frac{\mu}{100}$ because π is low. This implies $\angle(t_1, t_3) \leqslant \arcsin(\frac{\mu}{100}/\frac{2\mu}{6}) \leqslant 10°$. Thus we have $\angle(t_1, d_{\ell_q}), \angle(t_3, d_{\ell_q}) \leqslant 5°$. This implies $w(c_q) = d_2(T_1(c_q.x), T_2(c_q.y)) \leqslant \frac{1}{\cos(5°)} d_2(T_1(u_1.x), T_2(u_1.y)) \leqslant 1.01w(u_1)$. As $\angle(t_1, d_{\ell_q}), \angle(t_3, d_\ell) \leqslant 5°$, we get $w(d) \leqslant w(c_q) + 2\sin(5°)\lambda \max\{w(u_1), w(u_2)\} \leqslant (1.01 + 0.09\lambda) \max\{w(u_1), w(u_2)\}$.
  - $d_1(c_q, c) \leqslant 7 \max\{w(u_1), w(u_2)\}$: By $d_1(u_1, u_2) \leqslant 6 \max\{w(u_1), w(u_2)\}$ it follows that $d_1(u_1, c) \leqslant 6 \max\{w(u_1), w(u_2)\}$ holds. Furthermore, we have $d_1(u_1, c_q) \leqslant \sin(5°)w(u_1)$

because $\angle(d_{\ell_q}, t_1), \angle(d_{\ell_1}, t_3) \leqslant 5^\circ$. The triangle inequality implies $d_1(c, c_q) \leqslant d_1(c, u_1) + d_1(u_1, c_q) \leqslant 7 \max\{w(u_1), w(u_2)\}$.

  - $w(d) \leqslant 8.01 \max\{w(u_1), w(u_2)\}$ for all $d \in c_q c$: Above we already showed $w(c_q) \leqslant 1.01 w(u_1) \leqslant 1.01 \max\{w(u_1), w(u_2)\}$. By combining the 1-Lipschitz continuity of $w(\cdot)$ and $d_1(c_q, c) \leqslant 7 \max\{w(u_1), w(u_2)\}$ we obtain $w(d) \leqslant 8.01 \max\{w(u_1), w(u_2)\}$.

- $\lambda \geqslant 50$: Above we showed $d_1(c, u_1) \geqslant 6 \max\{w(u_1), w(u_2)\}$. The triangle inequality implies $d_1(u_1, a) + d_1(u_1, c) \geqslant d_1(a, c) \Rightarrow \lambda \max\{w(u_1), w(u_2)\} \geqslant (56 - 6) \max\{w(u_1), w(u_2)\}$.

- $|aa_1|_w, |aa_2|_w \geqslant 0.4874 \lambda^2 \max^2\{w(u_1), w(u_2)\}$: First we lower-bound $d_1(a, a_1), d_1(a, a_2) \geqslant 0.98 \lambda \max\{w(u_1), w(u_2)\}$: Above we already showed $d_1(u_1, c_q) \leqslant 0.09 \max\{w(u_1), w(u_2)\}$. Combining this with $d_1(u_1, a) = \lambda \max\{w(u_1), w(u_2)\}$ and the triangle inequality yields $d_1(a, c_q) \geqslant (\lambda - 0.09) \max\{w(u_1), w(u_2)\}$. Thus $d_1(a, a_1), d_1(a, a_2) \geqslant 0.98 \lambda \max\{w(u_1), w(u_2)\}$ because ℓ_q has a gradient of 1 and $\lambda \geqslant 50$.

  Above we already showed $w(a) \leqslant (1.01 + 0.09\lambda) \max\{w(u_1), w(u_2)\} \leqslant 0.12 \lambda \max\{w(u_1), w(u_2)\}$ because $\lambda \geqslant 50$. This implies $w(a_1) \geqslant d_1(a, a_1) - w(a) \geqslant 0.86 \lambda \max\{w(u_1), w(u_2)\}$ because $a.x = a_1.x$.

  By combining $w(a_1) \geqslant 0.86 \lambda \max\{w(u_1), w(u_2)\}$ and $d_1(a, a_1) \geqslant 0.98 \lambda \max\{w(u_1), w(u_2)\}$ we get $|aa_1|_w \geqslant 0.4874 \lambda^2 (\max\{w(u_1), w(u_2)\})^2$ as follows: Consider the subsegment $\overline{a}_1 a_1 := B_{0.86 \lambda \max\{w(u_1), w(u_2)\}}(a) \cap aa_1$. By $w(a_1) \geqslant 0.768 \lambda \max\{w(u_1), w(u_2)\}$ it follows $w(d) \geqslant 0.98 \lambda \max\{w(u_1), w(u_2)\} - d_1(a_1, d)$ for all $d \in \overline{a}_1 a_1$ because $w(\cdot)$ is 1-Lipschitz. This implies $|aa_1|_w \geqslant (0.3698 + 0.1176) \lambda^2 (\max\{w(u_1), w(u_2)\})^2 = 0.4874 \lambda^2 (\max\{w(u_1), w(u_2)\})^2$.

□

Lemma 13 implies that the approach taken in the proof of Lemma 10 yields that there is a path $\widetilde{\pi}_{qs} \subset G_2$ between q and s such that $|\widetilde{\pi}_{qs}|_w \leqslant (1 + \varepsilon) |\pi_{oqs}|_w$ If $d_1(u_1, u_2) < 6 \max\{w(u_1), w(u_2)\}$. Combining this with Lemmas 10 and 12 yields the following corollary:

Corollary 1 *Let $\widetilde{\pi} \subset G_2$ be a shortest path. We have $|\pi|_w \leqslant |\widetilde{\pi}|_w \leqslant (1 + \varepsilon) |\pi|_w$.*

3.3 "Bringing it all together"

In Subsections 3.1 and 3.2, we showed that in both cases, Case A and B, the minimum of the shortest path lengths in G_1 and G_2 is upper-bounded by $(1 + \varepsilon) |\pi|_w$, where π_w is a shortest path in P.

Next, we discuss that our algorithm has a running time of $\mathcal{O}(\frac{\zeta^4 n^4}{\varepsilon})$. Graph G_1 is given by the arrangement that is induced by $\Theta(\frac{\zeta^2 n^2}{\varepsilon})$ horizontal and $\Theta(\frac{\zeta^2 n^2}{\varepsilon})$ vertical lines because the corresponding grid has a mesh of size $\frac{\varepsilon \mu}{40000(|T_1| + |T_2|)}$. Thus, $|E_1| \in \Theta(\frac{\zeta^4 n^4}{\varepsilon^2})$. Graph G_2 is given by the arrangement that is induced by $\mathcal{O}(n^2)$ free space axis and $\Theta(n^2)$ grid balls. Each grid ball has a complexity of $\Theta(\frac{1}{\varepsilon})$. Thus, $|E_2| \in \mathcal{O}(\frac{n^4}{\varepsilon^2})$. Applying Dijkstra's shortest path algorithm on G_1 and G_2 takes time proportional to $\mathcal{O}(|E_1|)$ and $\mathcal{O}(|E_2|)$. As $|E_1| \in \Theta(\frac{\zeta^4 n^4}{\varepsilon^2})$ and $|E_2| \in \mathcal{O}(\frac{n^4}{\varepsilon^2})$ we have to ensure that each edge of $E_1 \cup E_2$ can be computed in constant time to guarantee an overall running time of $\mathcal{O}(\frac{\zeta^4 n^4}{\varepsilon^2})$.

Lemma 14 *All edges of G_1 and G_2 can be computed in $\mathcal{O}(1)$ time.*

Proof: There are two types of edges used in G_1 and G_2: (1.) axis aligned edges and (2.) edges that lie on a monotone free space axis. We consider both cases separately:

- Axis aligned edge $e \subset P$, see Figure 11(a): W.l.o.g., we assume that $e = (o, p)$ is horizontal. We have $|op|_w = \int_0^{|op|} w(o + t(o - p))\ dt = \int_{o.x}^{p.x} d_2(T_1(t), T_2(p.y))\ dt$, see Figure 11(a). Let $s \subset T_1$ be the segment such that $T_1(t) \in s$ for $t \in [p.x - o.x]$. W.l.o.g., we assume that s lies on the x-axis. $\int_{o.x}^{p.x} d_2(T_1(t), T_2(p.y))\ dt$ can be calculated as follows:

$$\begin{aligned}\int_{o.x}^{p.x} d_2(T_1(t), T_2(p.y))\ dt &= \int_{o.x}^{p.x} \sqrt{(T_1(t).x)^2 + (T_2(p.y).y)^2}\ dt \\ &= \frac{1}{2}\left(\begin{matrix} (T_2(p.y).y)^2 \operatorname{arsinh}\left(\frac{T_1(t).x}{T_2(p.y).y}\right) + \\ T_1(t).x\sqrt{(T_1(t).x)^2 + (T_2(p.y).y)^2} \end{matrix} \right)\Bigg|_{o.x}^{p.x}.\end{aligned}$$

  That value can be calculated in constant time.

- Edge e on a free space axis, see Figure 11(b): Let ℓ be the free space axis such that $e \subset \ell \subset P$ and $d_\ell \subset \mathbb{R}^2$ the corresponding angular bisector that corresponds to ℓ. By observation 2, we have $|op|_w = \int_0^{|op|} w(o + t(o - p))\ dt = \int d_2(T_1(t), T_2(t))\ dt$ where $T_1(t)T_2(t)$ lies perpendicular to d_ℓ, see Figure 11(b). Thus, $|op|_w$ is equal to the area that is bounded by $T_1(o.x)T_1(p.x)$, $T_2(o.y)T_2(p.y)$, $T_1(o.x)T_2(o.y)$, and $T_1(p.x)T_2(p.y)$ which can be computed in $\mathcal{O}(1)$ time.

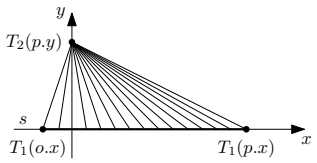

(a) Matching of a horizontal edge.

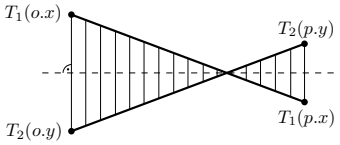

(b) Matching of an edge an a free space axis.

Figure 11: The two types of matchings that correspond to the two types of edges from G_1 and G_2.

□ This leads to our main result.

Theorem 1 *We can compute an $(1+\varepsilon)$-approximation of the integral Fréchet distance $\mathcal{F}_\mathcal{S}(T_1, T_2)$ in $\mathcal{O}(\frac{\zeta^4 n^4}{\varepsilon^2})$ time.*

4 Locally optimal Fréchet matchings

In this section, we discuss an application of Lemma 4 to so-called *locally correct (Fréchet) matchings* as introduced by Buchin et al. [4]. For $i \in \{1, 2\}$ and $0 \leqslant a \leqslant b \leqslant n$, we denote the subcurve between $T_i(a)$ and $T_i(b)$ by $T_i[a, b]$.

Definition 3 ([4]) *A matching (α_1, α_2) is* locally correct *if $\mathcal{D}(T_1[\alpha_1(a), \alpha_2(b)], T_2[\alpha_1(a), \alpha_2(b)]) = \max_{t\in[a,b]} d_2(T_1(\alpha_1(a)), T_2(\alpha_2(b)))$, for all $0 \leqslant a \leqslant b \leqslant n$.*

Buchin et al. [4] suggested to extend the definition of locally correct (Fréchet) matchings to "locally optimal" (Fréchet) matchings as future work. "The idea is to restrict to the locally correct matching that decreases the matched distance as quickly as possible."[4, p. 237]. To the best of our knowledge, such an extension of the definition of locally correct matchings has not been given until now. In the following, we give a definition of locally optimal matchings and show that each locally correct matching can be transformed, in $\mathcal{O}(n)$ time, into a locally optimal matching.

Buchin et al. [4] require the leash length to decrease as fast possible. In general though, there is no matching that ensures a monotonically decreasing leash length. We therefore also consider

increasing the leash length and extend the objective as follows: "Computing a locally correct matching that locally decreases and increases the leash length as fast as possible between two maxima". We measure how fast the leash length decreases (increases) as sum of the lengths of the subcurves that are needed to achieve a leash length of $\delta \geqslant 0$ (the next (local) maximum), then we continue from the point pair that realizes $\delta \geqslant 0$.

Thus, it seems to be natural to consider a matched point pair from $T_1 \times T_2$ in that a local maxima is achieved as fixed. Note that requiring a fast reduction and a fast enlargement of the leash length between two pairs $(T_1(\alpha_1(t_1)), T_2(\alpha_2(t_1)))$ and $(T_1(\alpha_1(t_2)), T_2(\alpha_2(t_2)))$ of fixed points is equivalent to requiring a matching that is optimal w.r.t. the partial Fréchet similarity between the curves between the points $T_1(\alpha_1(t_1))$ and $T_2(\alpha_2(t_1))$ and $T_1(\alpha_1(t_2))$ and $T_2(\alpha_2(t_2))$ for all thresholds $\delta \geqslant 0$.

In the following, we give a definition of locally correct matchings that considers the above described requirements. Let $f : [0, n] \to \mathbb{R}_{\geqslant 0}$. $t \in [0, 1]$, is the parameter of a *local maximum* of f if the following is fulfilled: there is a $\delta_t > 0$ such that for all $0 \leqslant \delta \leqslant \delta_t : f(t \pm \delta) \leqslant f(t)$ and $f(t+\delta) < f(t)$ or $f(t-\delta) < f(t)$. Given a matching (α_1, α_2), let $t_1, \ldots, t_k$ be the ordered sequence of parameters for all local maxima of the function $t \mapsto d_2(T_1(\alpha_1(t)), T_1(\alpha_1(t)))$. For any t_i, t_{i+1}, we denote the restrictions of α_1 and α_2 to $[t_i, t_{i+1}]$ as $\alpha_1[t_i, t_{i+1}] : [t_i, t_{i+1}] \to [\alpha_1(t_i), \alpha_1(t_{i+1})]$ and $\alpha_1[t_i, t_{i+1}] : [t_i, t_{i+1}] \to [\alpha_1(t_i), \alpha_1(t_{i+1})]$. We say (α_1, α_2) is *locally optimal* if it is locally correct and for all t_i, t_{i+1}, $\mathcal{P}_\delta(T_1[t_i, t_{i+1}], T_2[t_i, t_{i+1}]) = \mathcal{P}_{(\alpha_1[t_i,t_{i+1}],\alpha_2[t_i,t_{i+1}])}(T_1, T_2)$ for all $\delta \geqslant 0$.

By applying a similar approach as in the proof of Lemma 4 we obtain the following:

Lemma 15 *Let C be an arbitrarily chosen parameter cell and $a, b \in C$ such that $a \leqslant_{xy} b$ and π_{ab} the path induced by Lemma 4. Then, $\mathcal{P}_\delta(T_1[a.x, b.x], T_2[a.y, b.y]) = |\mathcal{E}_\delta \cap \pi_{ab}|$ for all $\delta \geqslant 0$, where $\mathcal{E}_\delta$ is the free space ellipse of C for the distance threshold δ.*

Lemma 15 implies that each locally correct matching π can be transformed into a locally optimal Fréchet matching in $\mathcal{O}(n)$ time as follows: Let $p_1, \ldots, p_{2n} \in \pi$ be the intersection points with the parameter grid. For each $i \in \{1, ..., 2n-1\}$ we substitute the subpath $\pi_{p_i p_{i+1}}$ by the path between p_i and p_{i+1} which is induced by Lemma 4. The algorithm from [4] computes a locally correct matching in $\mathcal{O}(n^3 \log n)$ time. Thus, a locally optimal matching can be computed in $\mathcal{O}(n^3 \log n)$ time.

5 Conclusion

We presented pseudo-polynomial $(1 + \varepsilon)$-approximation algorithms for the integral and average Fréchet distance which have a running time of $\mathcal{O}(\frac{\zeta^4 n^4}{\varepsilon^2})$. In particular, in our approach we compute two geometric graphs and their weighted shortest path lengths in parallel. It remains open if one can reduce the complexity of G_1 to polynomial with respect to the input parameters such that $G_1 \cup G_2$ still ensures an $(1 + \varepsilon)$-approximation.

References

[1] H.-K. Ahn, C. Knauer, M. Scherfenberg, L. Schlipf, and A. Vigneron. Computing the discrete Fréchet distance with imprecise input. *Int. J. Comput. Geometry Appl.*, 22(1):27–44, 2012.

[2] H. Alt and M. Godau. Computing the Fréchet distance between two polygonal curves. *Int. J. Comput. Geometry Appl.*, 5:75–91, 1995.

[3] S. Brakatsoulas, D. Pfoser, R. Salas, and C. Wenk. On map-matching vehicle tracking data. In K. Böhm, C. S. Jensen, L. M. Haas, M. L. Kersten, P.-Å. Larson, and B. C. Ooi, editors, *Proceedings of the 31st International Conference on Very Large Data Bases, Trondheim, Norway, August 30 - September 2, 2005*, pages 853–864. ACM, 2005.

[4] K. Buchin, M. Buchin, W. Meulemans, and B. Speckmann. Locally correct Fréchet matchings. In *ESA*, pages 229–240, 2012.

[5] K. Buchin, M. Buchin, and Y. Wang. Exact algorithms for partial curve matching via the Fréchet distance. In C. Mathieu, editor, *SODA*, pages 645–654. SIAM, 2009.

[6] M. Buchin. On the computability of the Fréchet distance between triangulated surfaces. Ph.D. thesis, Dept. of Comput. Sci., Freie Universität, Berlin, 2007.

[7] J.-L. D. Carufel, A. Gheibi, A. Maheshwari, J.-R. Sack, and C. Scheffer. Similarity of polygonal curves in the presence of outliers. *Comput. Geom.*, 47(5):625–641, 2014.

[8] A. Efrat, Q. Fan, and S. Venkatasubramanian. Curve matching, time warping, and light fields: New algorithms for computing similarity between curves. *Journal of Mathematical Imaging and Vision*, 27(3):203–216, 2007.

[9] J. Gudmundsson, P. Laube, and T. Wolle. Movement patterns in spatio-temporal data. In S. Shekhar and H. Xiong, editors, *Encyclopedia of GIS*, pages 726–732. Springer, 2008.

[10] J. Gudmundsson and N. Valladares. A GPU approach to subtrajectory clustering using the Fréchet distance. In *SIGSPATIAL/GIS*, pages 259–268, 2012.

[11] J. Gudmundsson and T. Wolle. Football analysis using spatio-temporal tools. In I. F. Cruz, C. A. Knoblock, P. Kröger, E. Tanin, and P. Widmayer, editors, *SIGSPATIAL/GIS*, pages 566–569. ACM, 2012.

[12] M. Jiang, Y. Xu, and B. Zhu. Protein structure-structure alignment with discrete fréchet distance. *J. Bioinformatics and Computational Biology*, 6(1):51–64, 2008.

[13] L. R. Rabiner and B.-H. Juang. *Fundamentals of speech recognition*. Prentice Hall Signal Processing series. Prentice Hall, 1993.

[14] E. Sriraghavendra, K. Karthik, and C. Bhattacharyya. Fréchet distance based approach for searching online handwritten documents. In *9th International Conference on Document Analysis and Recognition (ICDAR 2007), 23-26 September, Curitiba, Paraná, Brazil*, pages 461–465, 2007.

[15] S. Funke and E A. Ramos. Smooth-Surface Reconstruction in Near-Linear Time. In *Proceedings of the Thirteenth Annual ACM-SIAM Symposium on Discrete Algorithms*, pages 781–790, 2007.